# Dynamics of the Optically Directed Assembly and Disassembly of Gold Nanoplatelet Arrays

Delphine Coursault,[†] Nishant Sule,[†] John Parker,[†,‡] Ying Bao,[†,§,‖] and Norbert F. Scherer*,[†,§]

[†]James Franck Institute, University of Chicago, Chicago, Illinois 60637, United States
[‡]Department of Physics and [§]Department of Chemistry, University of Chicago, Chicago, Illinois 60637, United States
[‖]Department of Chemistry, Western Washington University, Bellingham, Washington 98225, United States

**S** *Supporting Information*
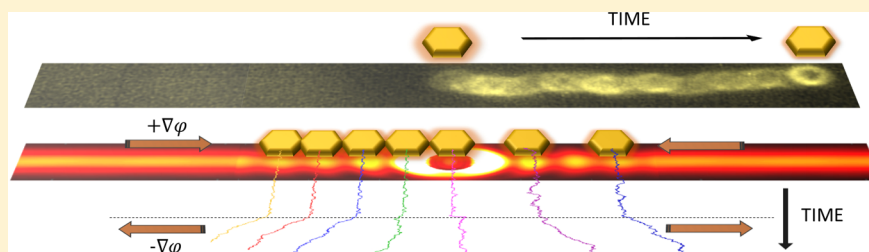
**ABSTRACT:** The tremendous progress in nanoscience now allows the creation of static nanostructured materials for a broad range of applications. A further goal is to achieve dynamic and reconfigurable nanostructures. One approach involves nanoparticle-based optical matter, but so far, studies have only considered spherical constituents. A nontrivial issue is that nanoparticles with other shapes are expected to have different local electromagnetic field distributions and interactions with neighbors in optical-matter arrays. Therefore, one would expect their dynamics to be different as well. This paper reports the directed assembly of ordered arrays of gold nanoplatelets in optical line traps, demonstrating the reconfigurability of the array by altering the phase gradient via holographic-beam shaping. The weaker gradient forces and resultant slower motion of the nanoplatelets, as compared with plasmonic (Ag and Au) nanospheres, allow the precise study of their assembly and disassembly dynamics. Both temporal and spatial correlations are detected between particles separated by distances of hundreds of nanometers to several microns. Electrodynamics simulations reveal the presence of multipolar plasmon modes that induce short-range (near-field) and longer-range electrodynamic (e.g., optical binding) interactions. These interactions and the interferences between mutipolar plamon modes cause both the strong correlations and the nonuniform dynamics observed. Our study demonstrates new opportunities for the generation of complex addressable optical matter and the creation of novel active optical technology.

**KEYWORDS:** *Optical trapping, electrodynamic coupling, plasmonics, optical matter, nanoparticle, multipole, nanoplatelet*

Creating persistent ordered nanostructures is an ongoing goal in nanoscience. Over the past decade, top-down and bottom-up fabrication and assembly approaches have matured impacting applications in nanophotonics,[1] sensing, and energy harvesting.[2,3] However, the research agenda is shifting toward achieving tunable, switchable, or nonlinear functionalities that require dynamic or reconfigurable nanostructures.[4−6] Optical matter, an assembly whose (nanoparticle) constituents are held together only by electromagnetic interactions,[7] offers tremendous opportunities to achieve this goal. However, this potential is only beginning to be explored and exploited.[8−11]

At the heart of optical matter is the concept of optical binding[9,12−14] of the constituent elements (e.g., dielectric colloids and plasmonic nanoparticles).[15−18] Whether in an incident plane wave or a shaped electromagnetic field, each (trapped) entity restructures the field creating forces that can cause more particles to be trapped and localized with wavelength-scale separations, creating ordered mesoscale assemblies. The controlled phase and amplitude shaping of

optical fields (for example, with spatial light modulators (SLMs)), allows the tailoring of optical forces to shape optical matter structures and drive their formation.[19−21] It has been shown that the polarization of the electromagnetic field affects the symmetry of the matter-field system, resulting in anisotropic forces and torques on spherical[22] and single anisotropic particles.[23−28] Optical binding interactions are thus very sensitive to light polarization,[13,14,17] which creates opportunities for directed assembly and the control of the dynamics in optical matter.[21] The localized surface plasmon resonance properties of Ag or Au nanoparticles increase their scattering cross-sections, thus enhancing electromagnetic interactions and propensity for nanoscale manipulation.[10,16,29] As a result, 1D, 2D, and 3D assemblies of spherical plasmonic
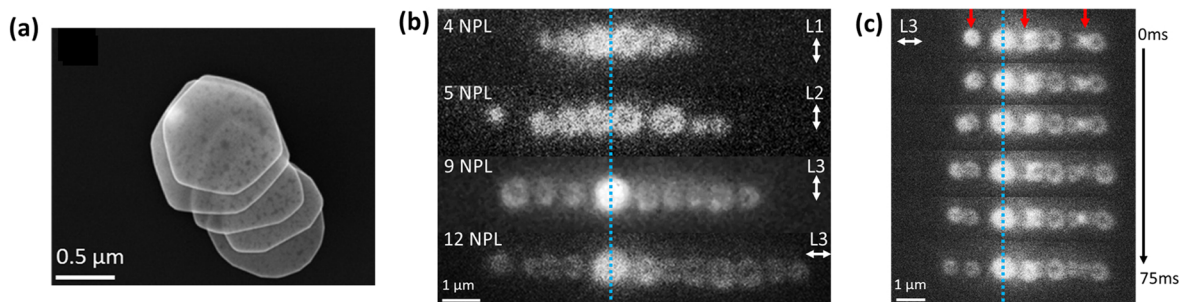
**Figure 1.** Shapes and sizes of Au NPLs and arrays in optical line traps. (a) TEM image of Au NPLs. (b,c) Dark-field optical microscopy images of Au NPL linear arrays in the line trap. The white double-headed arrows indicate the direction of light polarization in the optical traps. The blue dotted line indicates the position of the zero-order beam. In panel b, from L1 to L3, we observe formation of linear arrays with the number of NPLs increasing with the length of the line trap. In panel c, the red arrows point at the areas in which NPLs overlap; i.e., they stack on top of each other but do not stick to each other due to the Coulomb repulsion between their negatively charged PVP coating. The six images are successive frames from the video.

nanoparticles (as small as 40 nm) into optically bound arrays and supra-crystals have been achieved.[17,18,29]

New properties and novel dynamics are expected to emerge in optical matter constituted of anisotropic plasmonic nanoparticles due to enhanced anisotropic interactions, the increased significance of higher order (scattering) modes,[30] and potentially different or enhanced many-body effects. However, no experimental studies of optical binding or formation of optical matter from anisotropic (nano)particles have been reported. While near-field interactions have been investigated for small gold nanowires ($d/\lambda \ll 1$),[31,32] optical binding has only been investigated theoretically for cylindrical rods such as carbon nanotubes[14] or large dielectric nanorods, in which ladder-like structures with edge-to-edge optical binding separations have been predicted for a range of nanorod aspect ratios.[33] In addition, optical binding has mainly been described analytically[9,14] in terms of dipolar interactions. Therefore, it is of interest to elucidate the influence of higher-order scattering modes in directed assembly.

In this Letter, we demonstrate that highly anisotropic nano-objects, gold nanoplatelets (Au-NPLs) with an aspect ratio of ≥10, can form robust optical matter structures but with very different interactions and dynamics than nanospheres, as manifested both in the steady-state dynamics of the NPL arrays and during the assembly and disassembly process. We use SLM beam shaping of linearly polarized light to create optical line traps[18] and use them to investigate optical assembly of Au-NPLs in a quasi-1D geometry. The use of optical line traps allows the direct comparison of the influence of the phase gradient on NPLs to properties previously reported for plasmonic nanospheres.[18] For comparison, we also superimposed a Gaussian beam, the so-called zero-order, to the center of the line trap to further manipulate and stabilize NPL interactions, as manifested in NPL separations and fluctuations.

**Experimental Details.** In our optical trapping setup (see the schematic in the Supporting Information), the output from a cw Ti:sapphire laser at 70 mW power, measured before the objective, is directed to an inverted microscope (Olympus) and focused into a coverslip sandwich sample cell with a high-numerical-aperture water-immersion objective (NA = 1.2). The radiation pressure exerted by the laser beam pushes the PVP-coated NPLs toward the negatively charged top coverslip of the sample cell in which they are trapped near the water−glass interface. We use a spatial light modulator (Hamamatsu) to shape the Gaussian beam into a line trap by applying phase

masks that act as cylindrical lenses that can be either concave (type I; termed negative) or convex (type II; termed positive) (see Figure S1b). The beam's intensity distribution is Gaussian along both directions of the trap but of very different widths (Figure S1c), while the phase exhibits a parabolic distribution that is either negative (type I) or positive (type II) (Figure S1d). Consequently, the optical gradient force can be decomposed into two forces: (i) the intensity gradient force, which is the same for the two types of traps, and (ii) the phase gradient force, which is of opposite sign for type-I and type-II optical traps.[19,20] The balance between the forces depends on the particle's dielectric properties.[18] If the phase gradient dominates over the intensity gradient, particles can be driven directionally either into or out of the trap when the sign of the phase gradient is switched.[18]

In some experiments, we superimposed a focused Gaussian beam, the so-called "zero-order beam" onto the optical line trap to enhance the electromagnetic field at the center of the trap. When reflecting from the SLM, 5% of the incident Gaussian beam is not phase-modulated and becomes the so-called "zero-order" beam. The resulting line trap and zero-order beams are shown in the Supporting Information, while the consequences on NPL trapping are shown in Figure 1b.

**Results.** *Formation of Nanoplatelet Linear Arrays.* Figure 1a shows a transmission electron microscopy (TEM) image of Au-NPLs. The shape and diameter of NPLs vary, but on average, they are disk-like colloids with a diameter of 700 nm and a thickness of 25 nm.[34] Their synthesis leaves them negatively charged due to a coating of PVP molecules. Note that Au nanospheroids are also a product of the synthesis.

Viewed by dark-field microscopy (Figure 1b,c), NPLs appear as donut-like shapes with a bright corona around a dark central spot and have a weaker scattering intensity than 150−200 nm diameter Au (or Ag) nanospheres for the spectral detection window of the dark-field microscopy (450−750 nm). The NPLs are not only confined in the line trap but also oriented perpendicular to the beam propagation direction (and, hence, parallel to the coverslip). They organize into linear arrays for different optical trap configurations: (i) beams linearly polarized either parallel or perpendicular to the line trap axis, (ii) when the line trap and the Gaussian trap (zero-order beam) are superimposed (Figure 1b,c) or shifted from each other (see below), or both. The NPLs remain in linear (chain) configurations when the optical phase gradient is either negative, i.e., for an inward-directed phase gradient (type-I
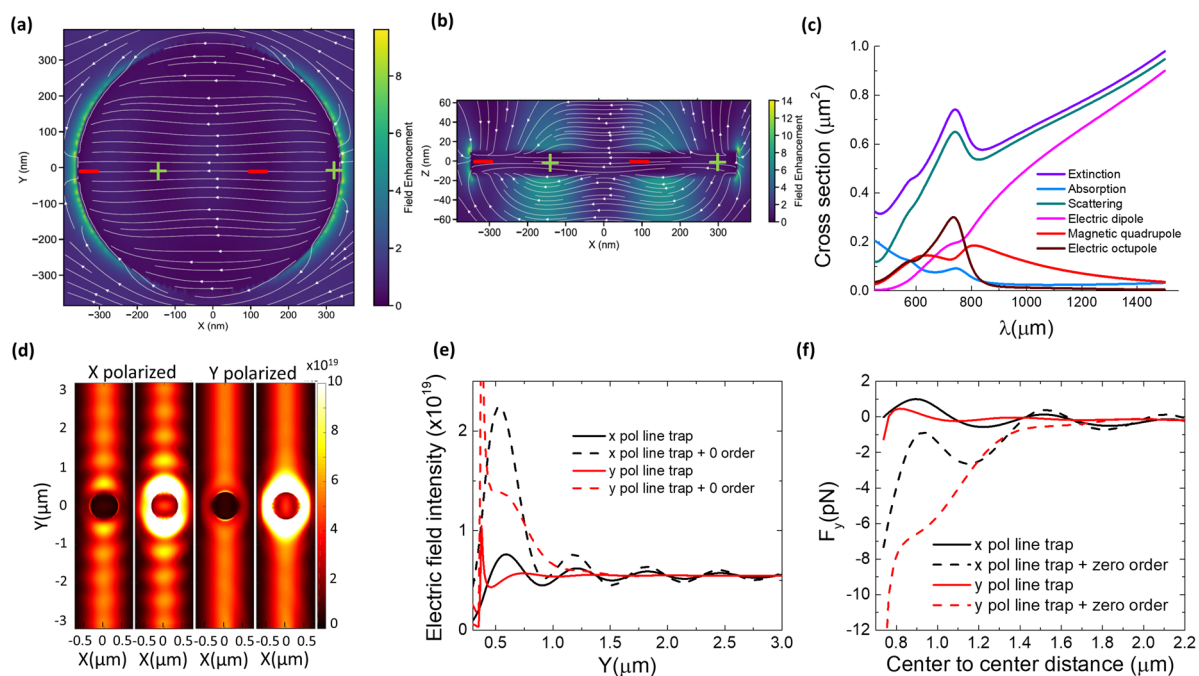
**Figure 2.** FDTD simulations of a Au NPL (assumed to be a disk of 700 nm in diameter and 25 nm in height) in a medium with $n = 1.33$ for water. (a, b) Map of the electric field enhancement at $\lambda = 800$ nm (vacuum) for incident light propagating along the $z$ direction and polarized along the $x$ axis; field enhancement and field lines (a) in the $XY$ plane, parallel to the plate, and (b) in the $XZ$ plane perpendicular to the NPL. (c) Total extinction, absorption, and scattering cross-sections with modal decomposition of the scattering cross-section. (d) 2D intensity map of the line trap with and without the presence of the zero-order beam with one NPL trapped at the center of the beam for a polarization direction parallel ($y$-polarized) or perpendicular to the line trap ($x$-polarized). (e) Electric-field intensity ($V^2/m^2$) along the line trap when a NPL is trapped at the center of the beam. (f) A comparison of the optical force along the $y$-axis when a NPL is trapped at the center of the line trap in the absence and presence of the zero-order beam.

trap) or positive, i.e., for an outward-directed phase gradient (type-II trap).

Figure 1b shows NPLs forming stable linear arrays in a type-I trap with array lengths increasing from 4 NPLs up to 12 NPLs. The NPLs are very close to one another and have an average center-to-center nearest neighbor distance that is essentially equal to their diameter ($d = 700$ nm) on average. As illustrated in Figure 1c, we observe variations of their scattered intensity that we attribute to two different phenomena: (i) fluctuations in their orientation and (ii) partial or full lateral overlap. Generally, the NPLs exhibit very small fluctuations of their orientation from perpendicularity to the incident beam's wavevector (see the Supporting Information). This is in agreement with previous results on high-aspect-ratio particles such as nanowires, in which the induced dipole tends to align with the polarization of the incident beam.[24] The NPLs can overlap laterally; that is, they can slide on top of one another and can even remain stably superimposed. The regions of partial overlap appear brighter in the dark-field images in Figure 1b,c. The red arrows in Figure 1c point to total or partial overlapping of NPLs. Partial overlap is less likely to occur when the polarization direction is perpendicular to the trap axis. It occurs more frequently when a NPL is already trapped by the zero-order beam and a newly trapped NPL is inserted into the array. Indeed, the NPLs tend to be stably fully overlapped when trapped at the zero-order location for both linear polarizations (parallel and perpendicular to the line trap axis).

These qualitative observations already show that the interactions between NPLs are different from what has been reported for either large colloids ($d/\lambda > 1$) or 200 nm Au nanospheres that are closer to the Rayleigh criterion. Strong

optical binding has been demonstrated for both micron-sized and submicron-sized particles with interparticle distances equal to multiples of the wavelength of the incident beam in the refractive index of the host medium.[9,13,16] Smaller plasmonic nanoparticles with diameters ranging from 40 to 200 nm can be organized on mesoscales, with center-to-center spacing equal to the wavelength of light in the medium; i.e., by optical binding. Electrodynamically bound dimers of spherical nanoparticles can form aligned parallel to the light polarization through near-field interactions.[17,35] Apparently, point dipole-like interactions are not sufficient to describe the interactions of NPLs in optical matter arrays. One should expect significant retardation associated with the large size of the NPL ($d/\lambda \approx 1$), resulting in more complex interactions than point-like dipole interactions that are suitable for describing optical-matter arrays created from smaller objects.

*Influence of Higher-Order Plasmon Modes.* We performed electrodynamics (finite-difference time domain, FDTD) simulations[22] to help understand why NPLs behave both similarly and differently than nanospheres. Figure 2a shows the calculated total field distribution in the NPL plane ($XY$ plane, $z = 0$). At first glance, the field resembles a dipole with strong enhancement at the edge of the NPL oriented parallel to the light polarization with an enhancement 2 to 9 times stronger than perpendicular to the polarization. However, a quadrupole-like enhancement pattern is also visible. This observation is evident in the $XZ$ plane (Figure 2b): the field enhancement shows two nodes and antinodes, and the phase changes sign 4 times over the NPL (see the Supporting Information). The quadrupole mode results from the retardation associated with the large size of the NPL.
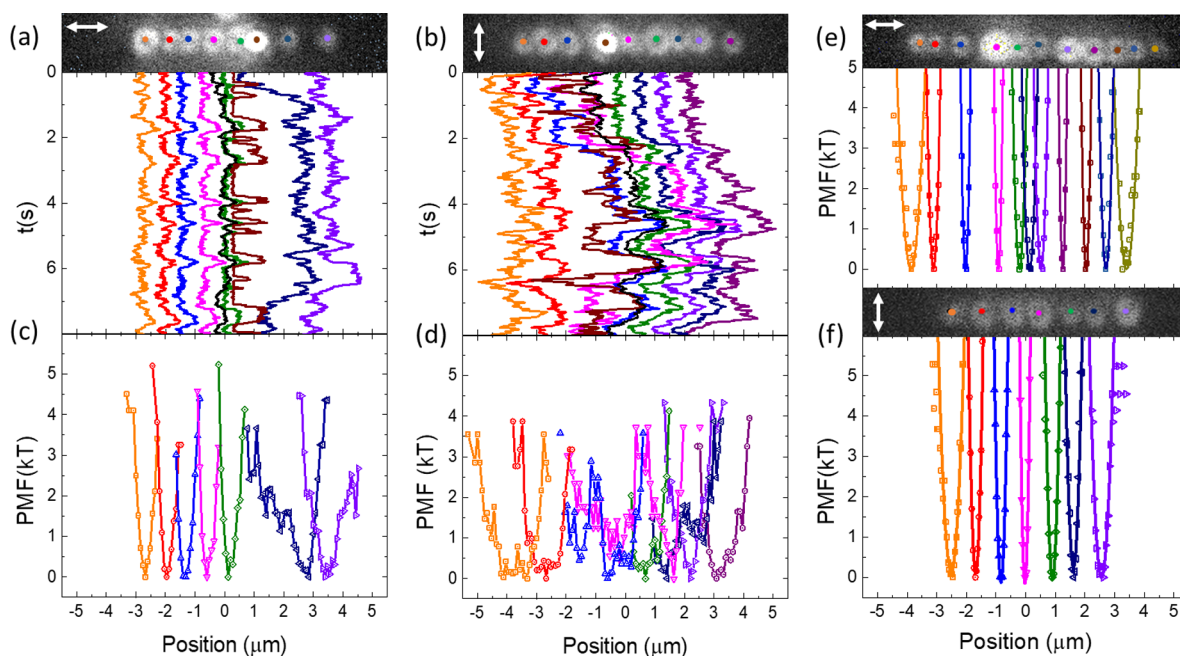
**Figure 3.** Dark-field images and time trajectories of the NPLs along the line trap. (a, b) In the absence of the zero-order beam for polarizations (a) parallel and (b) perpendicular to the NPL array. Colors are related to the position of the particle but do not imply identity of the NPL between the four experiments. The black and brown trajectories represent, respectively, the mean of the NPLs and that of a single Au nanosphere that was present in the array. (c, d) The potentials of mean force (PMFs) calculated from the probability density distributions of the time trajectories in the absence of the zero-order beam. (e, f) The PMFs of NPL arrays in the presence of the zero-order beam for both polarizations. NPL 4 (pink) is located at the position of the zero-order beam for both polarizations. The corresponding trajectories are shown in the Supporting Information. Symbols indicate experimental data, and solid lines indicate the corresponding harmonic fits (only shown in the presence of the zero-order beam; i.e., only in panels e and f).

The presence of high-order scattering modes is actually revealed by FDTD simulation using a spherical (versus cubical) flux box projecting onto multipolar basis functions (see the Supporting Information).[36] Figure 2c shows the extinction cross-section of a NPL that is dominated by the scattering contribution. A total of three multipolar plasmon modes are identified: a spectrally very broad electric dipole, a magnetic quadrupole, and an electric octupole. All 3 modes are excited at $\lambda = 800$ nm (the laser excitation wavelength in vacuum). Despite the dominance of the electric dipole, the magnetic quadrupole and the electric octupole modes cannot be neglected, as shown by the electric field distribution and the phase evolution, which are both very different compared to a dipole (Figure S7). Also, while the near-field enhancement remains maximized at the NPL edges parallel to the incident light polarization, it is increased in the presence of the higher order mode. As shown in the Supporting Information, when the octupole mode is resonant and dominant ($\lambda = 742$ nm), the enhancement is 10 times higher than in the presence of the dipole only ($\lambda = 1200$ nm). The multipole modes (and retardation) thus make important contributions to the near-field interaction between NPLs (Figure S7). The electric field distribution is highly polarized and explains why spatial overlapping of NPLs occurs, particularly when the polarization is parallel to the line trap direction, i.e., when the NPL array is aligned parallel to the polarization. Also the field lines across the NPL are parallel to the NPL plane and to the incident light polarization so that we expect stacking of NPLs to be stable, while the superimposed incident and scattered fields will be aligned and in-phase.

*Influence of the Optical Gradient and Zero-Order Focused Beam.* We also performed FDTD simulations to shed light on the optical binding interaction between the NPLs and the overlap phenomena at the location of the zero-order beam. The results are presented in Figure 2d−f. First, the optical line trap is simulated for both polarizations in the absence and presence of the zero-order beam with one NPL located at its center (Figure 2d,e). The light scattered by the NPL strongly interferes with the incident beam for a light polarization direction perpendicular to the line the trap, while the interference effect is very weak for the parallel polarization direction. This result is in agreement with the incident field interfering with the electric field radiated by a dipole; the maximum interference should occur at 90° to the orientation of the induced dipole. The electromagnetic field is strongly enhanced around and on top of the NPL in the presence of the zero-order beam for both polarizations. The amplitude of the first three interference antinodes is enhanced in the perpendicular polarization case. For parallel polarization, the enhancement decays to 0 on a similar length scale, around 2.4 μm away from the NPL center (i.e., 4 times the 600 nm trapping laser wavelength in water).

As illustrated in Figure 2f, this strong field enhancement gives rise to an enhanced optical gradient, resulting in a strong attractive force toward the center. In the absence of the zero-order beam and for parallel polarization, the near-field enhancement induces a strong and a very short-range attractive force; note that the minimum edge-to-edge distance is less than 60 nm between NPLs in the simulation. Only one stable equilibrium position is predicted for edge-to-edge distance of ∼255 nm (955 nm center-to-center). Because optical binding in nanospheres occurs at essentially integral multiples of the wavelength of light and this separation is only about half the incident wavelength, the nature of the interaction as either

**Table 1. Mean Center-to-Center Distance between the NPL in the Absence or Presence of the Zero-Order Beam**

| | | distances between NPL ($\mu$m) | | | | | | | | | |
|---|---|---|---|---|---|---|---|---|---|---|---|
| polarization | | 1–2 | 2–3 | 3–4 | 4–5 | 5–6 | 6–7 | 7–8 | 8–9 | 9–10 | 10–11 |
| // | A | 0.74 | 0.64 | 0.73 | 0.73 | | 0.57 | | | | |
| ⊥ | B | 0.84 | 0.87 | 1.13 | 1.1 | 0.75 | 0.77 | | 0.89 | | |
| // | C | 0.77 | 1.05 | 1.1[b] | 0.74[b] | 0.32 | 0.42 | 0.71 | 0.77 | 0.66 | 0.75 |
| ⊥ | D | 0.81 | 0.87 | 0.81[b] | 0.92[b] | 0.72 | 0.92 | | | | |

[a]A and B are without and C and D are with the zero-order beam. [b]NPL pairs closest to the position of the zero-order beam.

near-field, intermediate-scale, or both is more difficult to assess. In contrast, the electrodynamic interaction is repulsive in the absence of the zero-order beam over the same distance range for perpendicular polarization, and the first stable equilibrium position occurs at a edge-to-edge separation of 362 nm (1062 nm center-to-center), about $\lambda/2n$. There is a second stable position around 1700 nm center-to-center separation (about $3\lambda/2n$ edge-to-edge). This position in Figure 2f actually becomes the first stable position in the presence of the zero-order beam, while the shorter-distance interactions are now purely attractive. Therefore, because the measured inter-NPL spacings estimated from simulation and measured (see Figure3) are considerably smaller than $\lambda/4$, we conclude that near-field interactions are important in defining the structure of optical matter arrays of NPLs, particularly in the presence of the zero-order beam.

Both NPL interactions and inward-directed forces contribute to and cause the NPL stacking at the center of the trap in the presence of the zero-order beam. Conversely, only partial overlapping was observed in the absence of the zero-order beam (i.e., one NPL overlapped with two other NPLs at the center of the trap).

*Correlated Motions of NPLs in Linear Arrays at Steady State.* The optical field-induced stability of nanoplatelet arrays results from the NPL−optical trap interactions and the intra-array interactions (interactions between NPLs). The relative significance of each can be established by comparing the behavior of NPLs within the array at steady state in the absence and presence of the zero-order beam and for both polarizations parallel and perpendicular to the line trap.

We tracked the motions of the NPLs for the four trap configurations; i.e., both polarizations and with and without the zero-order beam. In Figure 3, each trapped NPL is represented by a different color. The center-to-center distances between the NPLs are comparable to their diameter for both polarizations (Table 1 and Figure 3) and are not strongly affected by the presence of the zero-order beam. On average, the inter-NPL distances are slightly smaller when the light polarization is parallel to the trap. This is in agreement with the expectation that a stronger near-field interaction would occur parallel to the polarization. For polarization perpendicular to the trap, the spacings of NPLs near the center of the trap and the location of the zero-order beam are consistent with the stable optical binding position determined from the FDTD simulation results shown in Figure 2f. In the absence of the zero-order beam, the NPLs at the center are separated by about 1.1 $\mu$m, corresponding to the first stable equilibrium center-to-center separation, while in the presence of the zero-order beam, the NPLs are nearly edge-to-edge. We notice that the center-to-center separations of NPL 4 with its second neighbors (NPLs 2 and 6) are close to 1.7 $\mu$m. All of the other spacings are nearly edge-to-edge, suggesting strong near-field interactions between

the NPLs in both the presence and the absence of the zero-order beam.

Panels a and b of Figure 3 show the tracked positions of an 8 NPL array and a 7 NPL array, respectively, formed in the absence of the zero-order beam for polarizations perpendicular (Figure 3a) and parallel (Figure 3b) to the trap. (An Au nanosphere (a side product of the synthesis) is also trapped near the center of the trap. It can laterally overlap with the NPLs but not get stuck to them.) The well-defined harmonic PMFs indicate constrained NPL motion observed in the trajectories of Figure 3 about "lattice sites". As mentioned above, the spacing values shown in Table 1 are consistent with our FDTD simulations. The force constants for the NPL motion about each site are given in Table 2.

In our experiment, we expect the intrinsic properties of both the trap (the optical intensity and phase gradients) and the NPLs (multipolar scattering) to affect any collective oscillations (modes) of the array. Because the trapping strength increases toward the trap center (see the Supporting Information) and the number of neighbors is different for each NPL due to the finite size of the system, the amplitude of the fluctuations around the mean position of each NPL should change with the particles' distance from the center of the trap. Also, the shape of the NPLs will affect how they scatter light and, therefore, the nature of their electrodynamic interactions and, thus, the transmission of a perturbation from site to site.

However, the main point is the extensive correlation of NPL motion observed in the trajectories of Figure 3. The strongly correlated motions of the NPLs suggest that NPL arrays behave like rigid bodies. This observation is in qualitative agreement with prior results obtained for small spherical nanoparticles.[18] In optical matter, oscillations of constituent particles about their mean locations have been described by analogy with phonons in a crystal lattice:[37] the lattice periodicity is dictated by the periodicity of the optical field, while oscillations are induced by small perturbations that lead to small displacements of the particles from their lattice site. At equilibrium (or steady state), the spectrum of fluctuations could be associated with a lattice temperature.[21] The displacements are transmitted from one particle to another via their electrodynamic interactions, but there could also be hydrodynamic interaction via the fluid (water).

Interestingly, the presence of the Au nanosphere disrupts the NPL array. It clearly induces an asymmetry in the array and causes large amplitude fluctuations in the NPL trajectories. Indeed, as shown Figure 3, each large jump observed in the sphere trajectory is followed by large amplitude fluctuations in the NPL trajectories. The closer the NPLs are to the nanosphere the stronger the perturbation (i.e., the larger the amplitude of NPL displacement). Moreover, the response of the NPLs to each perturbation is delayed by several tens of milliseconds, highlighting the different scales of forces associated with the two types of nano-objects.

**Table 2. Force Constants of NPLs from Harmonic Fits to PMFs of Figure 3**

| polarization | | mean | 1 | 2 | 3 | 4 | 5 | 6 | 7 | 8 | 9 | 10 | 11 |
|---|---|---|---|---|---|---|---|---|---|---|---|---|---|
| // | A | 0.04 | 0.07 | 0.09 | 0.09 | 0.01 | 0.1 | **0.01** | **0.02** | | | | |
| ⊥ | B | **0.01** | 0.01 | 0.02 | 0.01 | ∅ | 0.02 | ∅ | 0.02 | 0.02 | | | |
| // | C | 0.23 | 0.08 | 0.10 | 0.69 | 0.87 | 0.33 | 0.28 | 0.32 | 0.91 | 0.64 | 0.31 | 0.09 |
| ⊥ | D | 0.68 | 0.12 | 0.38 | 0.45 | 0.76 | 0.34 | 0.27 | 0.11 | | | | |

<sup>a</sup>A and B are without and C and D are with the zero-order beam. No value (∅) or only a rough estimation (bold text) of the force constant.

*Zero-Order Beam Stabilization of Optical Matter Arrays.* Given all of the aforementioned observations, the persistence of collective motions must imply that the interaction between the nanoplatelets is strong compared to $k_B T$ (with $k_B$, the Boltzmann constant and T the ambient temperature) and long-range. The trajectories (see the Supporting Information) show that the NPLs are more tightly trapped in the presence of the zero-order beam, which is particularly striking near the center of the trap. This is in agreement with FDTD simulations (Figure 2e), which show that interferences between the light scattered by the NPL and the optical trap are reinforced with the presence of the zero-order beam. Therefore, the collective oscillations observed in Figure 3 (and the Supporting Information) are of smaller amplitude with the zero-order beam because these NPLs are more tightly bound to their "sites". Despite some asymmetry of the assembly that is likely caused by the strong anchoring of one NPL at the zero-order location (whose position is shown by the pink color in Figure 3e,f), the arrays as a whole are more-stabilized by the presence of the zero-order beam.

The influences of the zero-order beam and the polarization on the stability and fluctuations of the NPL arrays can be quantified by the potential of mean force (PMF) of each individual NPL (Figure 3) and of the mean trajectory of each array (see the Supporting Information). Because the system of NPLs is at steady state (so long as no particles enter or leave the trap), we can determine the potential of mean force (PMF) confining the particle (NPL) from its probability density distribution, $\mathrm{PMF}(\{x\}_i) = -\ln[P(\{x\}_i)]$, where $\{x\}_i$ are the set of $x$ coordinate positions of particle i and $P(\{x\}_i)$ is the associated probability density distribution.

The trap stiffness for each individual NPL in each array is determined by fitting their associated PMF with a harmonic potential.[11] The confinement perpendicular to the trap (not shown) is about 10–20 fN/μm. The stiffness at their sites along the trap vary between approximately 10 to 100 fN/μm in the absence of the zero-order to 100 to 1000fN/μm (see Table 2). This is surprising because the increase of the total power due to the zero-order is only 5%. We attribute the increase of the stiffness by a factor of 10 for both polarizations in the presence of the zero-order beam to the associated enhanced fields and inter-NPL interactions (see Figure 2). The influence of the number of NPLs in the trap on the stiffness of the array is also a factor.

Both Figure 3e,f and Table 2 show that the NPL-associated PMFs become wider (i.e., smaller stiffness) as the distance from the mean position (0 μm) increases (see the Supporting Information). The increasing distance from the trap center also results in a decreasing number or total absence of neighbors on their outward side. This observation is in agreement with a decrease of the optical intensity and optical gradient force along the line;[18] both are enhanced by the presence of the zero-order beam (Figure 2d). Their enhancements lead to stronger inter-

NPL interactions that stabilize the overall array and each NPL in it. This conclusion is most dramatic when one NPL is strongly anchored at the zero-order location (shown in pink in Figure 3e,f). In one case, the center of the trap overlaps with the center the array (Figure 3f). In the other case, because it is an asymmetric assembly, the zero-order beam did not overlap the array center. The NPL at the zero-order position acts like a barrier that disconnects the motion of the NPL on each side (see the Supporting Information). The induced electrodynamic asymmetry will require further investigation and is beyond the scope of this paper.

Finally, we note that when the NPL array was disrupted by the presence of a Au nanosphere, the probability density distribution of the closest NPL departed from the expected Gaussian shape becoming either a strongly skewed Gaussian distribution (Figure 3c) that leads to an asymmetric PMF or a very broad distribution (Figure 3d), leading to multiple shallow wells in the PMF. In these cases, either no value or only a rough estimation of the stiffness (bold) is given in Table 2.

*Influence of the Phase Gradient on NPL Dynamics.* Figure 4a shows consecutive snapshots (images) of the NPLs in a type-II trap in which the phase gradient is opposite to the intensity gradient; that is, the phase gradient pushes the Au nanosphere and the Au NPLs out of the line trap along its main axis. The green arrows point at the single rapidly moving Au nanosphere that had been trapped together with the Au NPLs. The Au nanosphere is driven more than 10 times faster than the outermost nanoplatelet. The much-slower motion of NPLs shows that they are much less responsive to the phase gradient than the Au nanospheres.

The different dynamics of NPLs and Au nanospheres would be affected by electrodynamic forces, hydrodynamic and frictional drag, and thermal gradients and fluid flow. Despite an estimated temperature increase of the NPL of 100 °C,[38] thermal transport calculations show that the heat should be rapidly dissipated into the glass and the temperature of the NPL decreased by roughly 1 order of magnitude.[39] Thus, neither the viscosity nor the fluid flow should be strongly affected when the NPLs are so close to the glass–water interface; the induced inward flow should be less 10 nm/s.[40]

We calculated the translational drag coefficient for a NPL oriented with its short axis perpendicular to the motion to determine whether hydrodynamic drag forces may be responsible for the slower motion of the NPLs. According to Perrin's formula,[41] the friction coefficient for a disk of height of $a = 25$ nm and a radius of $b = 350$ nm immersed in water ($\eta_{H_2O} = 10^{-3}$ Pa.s), $\gamma_{NPL} = 0.66 \times 10^{-12}$ (N·s)/m versus $\gamma_{NP} = 2 \times 10^{-}$ (N·s)/m for a 200 nm diameter nanosphere. Thus, assuming equal electrodynamic forces, the hydrodynamics suggest that a nanosphere would move $10^3$–$10^4$ times slower than a NPL. A correction of the viscous drag coefficient that takes into account the distance to the substrate would increase the NPL drag by 1
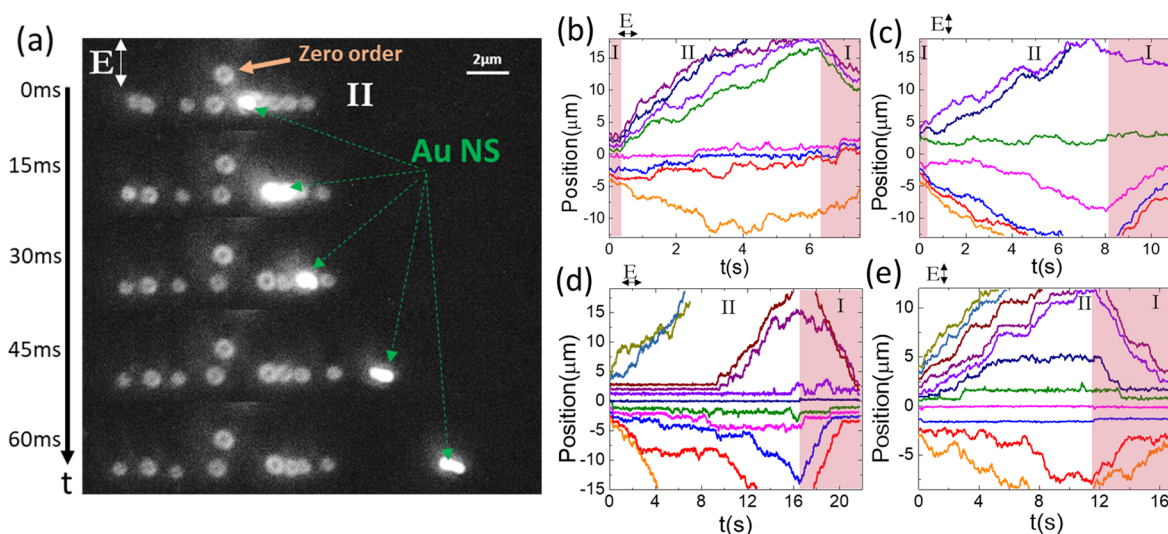
**Figure 4.** Driven dynamics of NPLs in line traps. (a) Successive dark-field images of NPLs and a single nanosphere driven out of the trap. Time trajectories of NPLs driven along the main axis in a type-II and then a type-I trap (shaded regions), respectively, for perpendicular and parallel polarization in the absence (panels b and c) and presence (panels d and e) of the zero-order beam. Note that the shape of the Au nanosphere (Au NS) is elongated due to its rapid motion during the 15 ms acquisition time per frame.

order of magnitude[42] (see the Supporting Information). Therefore, we conclude that the main cause for difference in the motion of NPLs and Au nanospheres results come from the electrodynamic forces, confirming insights from our FDTD simulations that the NPLs interact very differently with light than do nanospheres. We inverted the phase gradient (type-II trap) after NPLs are organized into one-dimensional arrays and then waited 6−16 s and reversed the phase gradient again to a type-I trap to measure their collective dynamics during disassembly and assembly. This procedure, as shown in Figure 4b−e, drives the NPLs outward (type-II trap) or inward (type-I trap) along the main axis of the line trap. The influence of the zero-order beam is revealed when it is shifted away from the line trap. We study the dynamics for parallel and perpendicular polarizations.

As shown in Figure 4a, the traps are rapidly cleared of incidental Au nanospheres owing to the slower drift of the NPLs, thus allowing unperturbed measurements of NPL interactions and dynamics. The trajectories of the NPLs shown in Figure 4b,c reveal nonmonotonic and time-correlated drift. Despite the differences in the trajectories of the individual NPLs, there are several general or common features. First, the closer the NPLs are to the center, the longer it takes them to escape. Second, we observed that in most cases the most central NPLs did not escape and remained close to the center during the whole experiment. Third, when the NPLs were driven outward, they escape the trap (type-II trap) at slower speed than when they are driven toward the center (type-I trap). The last observation is consistent with the fact that the intensity and phase gradients are in the same (type I) direction or opposite (type II) directions and act synergistically or antithetically, respectively.

With regard to the particulars, in the case of only a single trapped NPL (see the Supporting Information), we observed that once the NPL escaped the trap center (type II), it moved at a constant speed, similar to the case of single nanospheres but slower.[18] In contrast, when multiple NPLs are trapped, portions of the single NPL trajectories appear to be highly correlated with neighbors; e.g., several NPLs move in near-lock-

step in panels b−e, exhibit halting plateau-like correlated motions as in panel e, or both. The drift of each NPL appears altered according to the number of neighboring NPLs, the distance between them, and their position in the trap. The correlated drift is due to electrodynamic interactions between NPLs and with the spatially structured field in optical trap (see Figure 2d). We expect the hydrodynamic interactions between NPLs to play a minor role, particularly as it was recently shown that electrodynamic interactions can be dominant over hydrodynamic in light-driven plasmonic nanoparticle systems.[21]

Nevertheless, it is very surprising to observe correlation between the NPLs when they are more than 10 μm away from the trap center. The effect is even more striking in the presence of the zero-order beam (Figure 4d,e); there are not only time correlations between the trajectories but also spatial correlations with the NPLs pausing at regular distances from the center of trap when they are driven. We believe that the interferences between incident and scattered light sculpt the potential landscape in situ over tens of micrometers. These correlated and spatially structured dynamics offer a new opportunity for tuning particle transport.

In addition, the manipulation of the light polarization should allow the control of the one-by-one release of the NPLs. The two polarizations studied induced different dynamics, and their effects are enhanced by the presence of the zero-order beam. For polarization parallel to the trap, the escape of the NPL is easier (faster), but their drift is not constant. For perpendicular polarization, the NPLs remain anchored to the trap center for a longer time (some even did not have time to escape during our experiment), but their trajectories are smoother as they escape. Our FDTD simulations of Figure 2 revealed the enhancement of the electric field intensity when a NPL is trapped at the location of the zero-order beam. Electrodynamic−Langevin dynamic[22] results for 2 NPLs shown in the Supporting Information recapitulate the step-like trajectories observed in the experiment, but the aspect ratio and irregular shape of the NPLs make the simulations very challenging. In the optical line, we expect the enhancement to increase by adding more NPLs because their mutual scattering increases the field intensity at

the location of their neighbors, an optical binding phenomenon.[43]

**Summary and Conclusions.** We trapped and oriented anisotropic disk-like Au NPLs in optical line traps. The unique electrodynamic interaction between the NPLs and their dynamics depend on their arrangement with respect to the polarization direction of the incident beam compared to the trap axis and the presence and absence of an intense and tightly focused zero-order beam. Switching the sign of the optical phase gradient drives the assembly or disassembly of the NPL arrays over distances of tens of microns. Because NPLs exhibit significantly slower transport compared with plasmonic nanospheres due to their specific multipolar excitations, we are able to controllably clear contaminating nanospheres from the line trap, revealing highly correlated motions at steady state and during the transient assembly and disassembly processes. These correlations reflect near-field and optical-binding-type interactions of the NPLs and the optical trap, as supported by results of our FDTD simulations. In particular, the superposition of a focused Gaussian beam at the center of the line trap stabilizes the long NPL linear arrays and strongly influences the long-range spatial correlations of their motions during assembly and disassembly through long-range retarded dipolar interactions.

These findings are surprising and are not mere extensions of recent reports on the importance of the optical phase gradient force in controlling optical matter.[18,20] To our knowledge, there have been no similar observations of correlated drift reported for plasmonic nanospheres. If analogous correlated drift occurs in the driven dynamics of nanospheres, its observation will require much -higher frame rates or more-viscous solution conditions to measure. In fact, we expect the collective drift phenomenon to be somewhat unique to NPLs (and perhaps other higly anisotropic nanoparticles[33]) because the multipolar excitations and the interactions inherent therein create a more-complex potential energy landscape. The separations of the NPLs summarized in Table 1 are not values typical of optical binding ($d \approx \lambda/n$ with $\lambda = 800$ nm and $n = 1.33$, leading to $d \approx$ 600 or 1200 nm), whereas nanospheres are dominantly separated by such well-defined distances or at near-field separations.[13,17,18] Simulations coupling electrodynamics and Langevin dynamics[22] could shed light on how the collective dynamic of multiple NPLs reshape the optical field and optical trap and, more specifically, how the symmetry of the assembly influences the NPL dynamic on each side of the trap center.

Our findings expand the ways to manipulate plasmonic nanoparticle by exploiting temporal and spatial correlation between particles separated by hundreds of nanometers to a few microns. It opens opportunities for exploiting multipolar plasmon modes with which to sculpt light with nanoscale precision over tens of micrometers and for creating laser-printed nanoparticle structures on substrates.

## ASSOCIATED CONTENT

### Ⓢ Supporting Information

The Supporting Information is available free of charge on the ACS Publications website at DOI: 10.1021/acs.nanolett.8b00199.

> NPLs trapped in a type I trap: the polarization of the incident beam is switched between linear and elliptical polarization with a period of 5 seconds. The video was recorded at 65 fps. (AVI)

The NPL array is formed in a type I optical line trap with linear polarization perpendicular to the trap. A Gaussian beam is superimposed to the center of the optical line trap. The video was recorded at 65 fps. (AVI)

The NPL array is formed in a type I optical line trap with linear polarization parallel to the trap. A Gaussian beam is superimposed to the center of the optical line trap. The video was recorded at 65 fps. (AVI)

The NPL array is formed in a type I optical line trap with linear polarization perpendicular to the trap. The phase gradient is first inverted and the NPLs are driven linearly out of trap (type II trap) then the phase gradient is again reversed (type I trap). A Gaussian beam is shifted from the center of the line trap. The video was recorded at 65 fps. (AVI)

The NPL array is formed in a type I optical line trap with linear polarization parallel to the trap. The phase gradient is first inverted and the NPLs are driven linearly out of trap (type II trap) then the phase gradient is again reversed (type I trap). A Gaussian beam is shifted from the center of the line trap. The Video was recorded at 65 fps. (AVI)

The NPL array is formed in type I optical line trap with linear polarization perpendicular to the trap. Then the NPLs are driven linearly out of trap by inverting the phase gradient (type II trap) and driven in again (type I trap). A Gaussian beam is superimposed to the center of the optical line trap. The video was recorded at 65 fps. (AVI)

The NPL array is formed in a type I optical line trap with linear polarization parallel to the trap. The phase gradient is first inverted and the NPLs are driven linearly out of trap (type II trap) then the phase gradient is again reversed (type I trap). A Gaussian beam is superimposed to the center of the optical line trap. The video was recorded at 65 fps. (AVI)

A single NPL is trapped in a type I optical line trap with linear polarization perpendicular to the trap. Then the NPL is driven linearly out of trap by inverting the phase gradient (type II trap). The video was recorded at 33 fps. (AVI)

Details on experimental and electrodynamic simulation methods and calculations. Figures showing an optical trapping and dark-field microscopy system, phase masks, measured phase profiles, beam microscopy images, NPL rotation and trajectories, the potential of mean force of NPLs at the steady state, single-NPL-driven motion, calculated viscous drag coefficient correction, FDTD simulations, and simulated trajectories. (PDF)

## AUTHOR INFORMATION

**Corresponding Author**

*E-mail: nfschere@uchicago.edu.

**ORCID** Ⓞ

Delphine Coursault: 0000-0002-0051-5376

**Notes**

The authors declare no competing financial interest.

## ■ REFERENCES

(1) Monticone, F.; Alù, A. *Rep. Prog. Phys.* **2017**, *80*, 036401.

(2) de Aberasturi, D. J.; Serrano-Montes, A. B.; Liz-Marzán, L. M. *Adv. Opt. Mater.* **2015**, *3*, 602−617.

(3) Atwater, H. A.; Polman, A. *Nat. Mater.* **2010**, *9*, 205−213.

(4) McEvoy, M. A.; Correll, N. *Science* **2015**, *347*, 1261689.

(5) Fan, X.; Chung, J. Y.; Lim, Y. X.; Li, Z.; Loh, X. J. *ACS Appl. Mater. Interfaces* **2016**, *8*, 33351−33370.

(6) Ong, L. L.; et al. *Nature* **2017**, *552*, 72.

(7) Burns, M. M.; Fournier, J.-M.; Golovchenko, J. A. *Science* **1990**, *249*, 749.

(8) Dienerowitz, M.; Mazilu, M.; Dholakia, K. *J. Nanophotonics* **2008**, *2*, 021875−021875−32.

(9) Dholakia, K.; Zemánek, P. *Rev. Mod. Phys.* **2010**, *82*, 1767−1791.

(10) Yan, Z.; Bao, Y.; Manna, U.; Shah, R. A.; Scherer, N. F. *Nano Lett.* **2014**, *14*, 2436−2442.

(11) Jones, P. H.; Maragò, O. M.; Volpe, G. *Optical Tweezers: Principles and Applications*; Cambridge University Press: Cambridge, U.K., 2015.

(12) Thirunamachandran, T. *Mol. Phys.* **1980**, *40*, 393−399.

(13) Burns, M. M.; Fournier, J.-M.; Golovchenko, J. A. *Phys. Rev. Lett.* **1989**, *63*, 1233−1236.

(14) Bradshaw, D. S.; Andrews, D. L. *Phys. Rev. A: At., Mol., Opt. Phys.* **2005**, *72*, 033816.

(15) Righini, M.; Zelenina, A. S.; Girard, C.; Quidant, R. *Nat. Phys.* **2007**, *3*, 477.

(16) Demergis, V.; Florin, E.-L. *Nano Lett.* **2012**, *12*, 5756−5760.

(17) Yan, Z.; Gray, S. K.; Scherer, N. F. *Nat. Commun.* **2014**, *5*, 3751.

(18) Yan, Z.; Sajjan, M.; Scherer, N. F. *Phys. Rev. Lett.* **2015**, *114*, 143901.

(19) Grier, D. G. *Nature* **2003**, *424*, 810−816.

(20) Roichman, Y.; Sun, B.; Roichman, Y.; Amato-Grill, J.; Grier, D. G. *Phys. Rev. Lett.* **2008**, *100*, 013602.

(21) Figliozzi, P.; Sule, N.; Yan, Z.; Bao, Y.; Burov, S.; Gray, S. K.; Rice, S. A.; Vaikuntanathan, S.; Scherer, N. F. *Phys. Rev. E: Stat. Phys., Plasmas, Fluids, Relat. Interdiscip. Top.* **2017**, *95*, 022604.

(22) Sule, N.; Rice, S. A.; Gray, S. K.; Scherer, N. F. *Opt. Express* **2015**, *23*, 29978−29992.

(23) Pelton, M.; Liu, M.; Kim, H. Y.; Smith, G.; Guyot-Sionnest, P.; Scherer, N. F. *Opt. Lett.* **2006**, *31*, 2075−2077.

(24) Tong, L.; Miljković, V. D.; Käll, M. *Nano Lett.* **2010**, *10*, 268−273.

(25) Yan, Z.; Scherer, N. F. *J. Phys. Chem. Lett.* **2013**, *4*, 2937−2942.

(26) Messina, E.; Donato, M. G.; Zimbone, M.; Saija, R.; Iatì, M. A.; Calcagno, L.; Fragalà, M. E.; Compagnini, G.; D'Andrea, C.; Foti, A.; Gucciardi, P. G.; Maragò, O. M. *Opt. Express* **2015**, *23*, 8720−8730.

(27) Brzobohatý, O.; Šiler, M.; Trojek, J.; Chvátal, L.; Karásek, V.; Zemánek, P. *Opt. Express* **2015**, *23*, 8179−8189.

(28) Liaw, J.-W.; Lo, W.-J.; Lin, W.-C.; Kuo, M.-K. *J. Quant. Spectrosc. Radiat. Transfer* **2015**, *162*, 133−142 Laser-light and Interactions with Particles 2014.

(29) Yan, Z.; Shah, R. A.; Chado, G.; Gray, S. K.; Pelton, M.; Scherer, N. F. *ACS Nano* **2013**, *7*, 1790−1802.

(30) Liu, W.; Kivshar, Y. S. *Philosophical Transactions of the Royal Society of London A: Mathematical, Physical and Engineering Sciences* **2017**, *375* (2090), 1.

(31) Zhao, R.; Tassin, P.; Koschny, T.; Soukoulis, C. M. *Opt. Express* **2010**, *18*, 25665−25676.

(32) Ekeroth, R. M. A. *J. Opt.* **2016**, *18*, 085003.

(33) Simpson, S. H.; Zemánek, P.; Maragó, O. M.; Jones, P. H.; Hanna, S. *Nano Lett.* **2017**, *17*, 3485−3492.

(34) Viarbitskaya, S.; Teulle, A.; Marty, R.; Sharma, J.; Girard, C.; Arbouet, A.; Dujardin, E. *Nat. Mater.* **2013**, *12*, 426−432.

(35) Sule, N.; Yifat, Y.; Gray, S. K.; Scherer, N. F. *Nano Lett.* **2017**, *17*, 6548−6556.

(36) Parker, J.; Gray, S.; Scherer, N. 2017, arXiv:1711.06833. arXiv.org e-Print archive. http://adsabs.harvard.edu/abs/2017arXiv171106833P (accessed Dec 7, 2017).

(37) de Abajo, F. J. G. *Opt. Express* **2007**, *15*, 11082−11094.

(38) Baffou, G.; Quidant, R.; García de Abajo, F. J. *ACS Nano* **2010**, *4*, 709−716.

(39) Baffou, G.; Quidant, R.; Girard, C. *Phys. Rev. B: Condens. Matter Mater. Phys.* **2010**, *82*, 165424.

(40) Donner, J. S.; Baffou, G.; McCloskey, D.; Quidant, R. *ACS Nano* **2011**, *5*, 5457−5462.

(41) Perrin, F. *J. Phys. Radium* **1934**, *5*, 497−511.

(42) Kim, M.-U.; Kim, K. W.; Cho, Y.-H.; Kwak, B. M. *Fluid Dynamics Research* **2001**, *29*, 137.

(43) Rodríguez, J.; Dávila Romero, L. C.; Andrews, D. L. *Phys. Rev. A: At., Mol., Opt. Phys.* **2008**, *78*, 043805.